Serine^{92} (F7) Contributes to the Control of Heme Reactivity and Stability in Myoglobin†

Stephen J. Smerdon,‡ Szymon Krzywda, and Anthony J. Wilkinson*

Department of Chemistry, University of York, Heslington, York YO1 5DD, U.K.

Robert E. Brantley, Jr., Theodore E. Carver,§ Mark S. Hargrove, and John S. Olson

Department of Biochemistry and Cell Biology and the W. M. Keck Center for Computational Biology, Rice University, Houston, Texas 77251

Received December 16, 1992

ABSTRACT: The effects of mutation of the conserved serine^{92} residue to alanine, valine, and leucine in pig myoglobin have been determined. In myoglobin crystal structures, the hydroxyl group of serine^{92} is within hydrogen-bonding distance of the N_δ-H of histidine^{93}, whose N_ϵ coordinates the iron atom of the heme prosthetic group. The association equilibrium constants of the ferrous forms of the mutant myoglobins for O_2, CO, and methyl and ethyl isocyanide are increased 1.3–13-fold relative to the wild-type protein. The rates of azide association with the mutant ferric proteins at neutral pH are decreased by factors of 2–5 consistent with an increased affinity for the iron-bound water molecule which must be displaced. The dissociation rates for azide appear to be decreased 4–10-fold, suggesting that the affinity of the mutant proteins for this ligand is also higher. Thus, the overall affinities are increased regardless of the chemical nature of the liganded species, indicating that the reactivity of the heme iron itself has been raised. Time courses for association of methyl and ethyl isocyanide at high concentrations show fast and slow phases in which the absorbance at 445 nm drops and then rises, respectively. Comparison of these traces with spectra following the reaction of isocyanide ligands with chelated proton heme in soap micelles indicates that the slow phase is associated with the breaking of the iron–proximal histidine bond and the binding of a second isocyanide species in the proximal heme pocket. The rates of hemin dissociation from the Ala^{92} and Leu^{92} mutants are 10–20-fold faster than that for the wild-type protein at pH 5. The X-ray structure of the aquomet form of the Leu^{92} mutant has been solved to a nominal d_{min} = 2.7 Å. Hydrogen-bonding and electrostatic interactions involving residue^{92}, the proximal histidine, the heme-7-propionate, and histidine^{97} have been disrupted, leading to a more exposed proximal heme pocket which allows access of the second isocyanide ligand and lowers the stability of the heme with respect to dissociation.

The role of protein side chains in controlling the affinity of mammalian hemoglobins and myoglobins for ligands has been a target of much study over many years. Recently, site-directed mutagenesis has been used, in combination with kinetic and equilibrium studies of ligand binding and X-ray crystallographic analysis, to delineate the functional importance of key residues on the distal side of the heme group (Nagai et al., 1987; Olson et al., 1988; Springer et al., 1989; Mathews et al., 1989; Egeberg et al., 1990; Carver et al., 1991; Smerdon et al., 1991). This work has allowed the contributions that individual side chains make to the ligand binding kinetics and equilibria to be evaluated in both proteins. These experiments have also confirmed that for hemoglobin β-subunits, changes in the distal pocket structure which accompany the T- to R-state allosteric transition are responsible for the increased reactivity in the R-state (Liddington et al., 1988; Mathews et al., 1991). Less attention has so far been paid to the role of residues on the proximal side of the heme in the control of the ligand binding process. The accessibility of the iron, and hence its reactivity toward ligands, is determined by its coordination geometry with the pyrrole nitrogens in the porphyrin ring and the nitrogen of the proximal histidine (F8). Restraints that maintain the iron out of the plane of the pyrrole nitrogens are believed to be responsible for the lowered reactivity of T-state α-subunits in hemoglobin (Perutz, 1970; Liddington, et al., 1988; Mathews et al., 1991).

In pig myoglobin, the N_δ-H of His^{93} makes a bifurcated hydrogen bond with the main-chain >C=O group of Leu^{89} (F4) and Oγ of Ser^{92} (F7); a similar organization exists in sperm whale myoglobin and has been noted in horse myglobin (Oldfield et al., 1992; Evans & Brayer, 1990). These residues form part of a hydrogen-bonding lattice extending from His^{93} to the heme-7-propionic acid group and the imidazole of histidine^{97} (FG2) on the protein surface (Figure 1). The conformation of the His^{93} imidazole appears to be tightly constrained by these interactions. As a result, the plane of the imidazole eclipses the equatorial Fe–Np bonds of pyrroles A and C (Figure 1, bottom). This conformation is sterically unfavorable owing to the close contact of the pyrrole nitrogens with the C_ϵ and C_δ imidazole ring carbons, 3.10 and 3.09 Å, respectively. Calculations have suggested, however, that, relative to the staggered orientation, the eclipsed conformation is favored by electronic effects, possibly accounting for the propensity of the imidazole ligands of model heme compounds to adopt intermediate geometries (Scheidt & Chipman, 1986).

† Supported by Grant GR/E 98867 from the Science and Engineering Research Council, U.K., U.S. Public Health Service Grants GM-35649 and HL-47020, Grant C-612 from the Robert A. Welch Foundation, and the W. M. Keck Foundation.

‡ Present address: Department of Molecular Biophysics and Biochemistry, Yale University, New Haven, CT 06511.

§ Recipient of a graduate fellowship from the National Institutes of Health Training Grant GM-08280. Present address: Department of Molecular Biology, Scripps Research Institute, La Jolla, CA 92037-9701.

0006-2960/93/0432-5132$04.00/0 © 1993 American Chemical Society

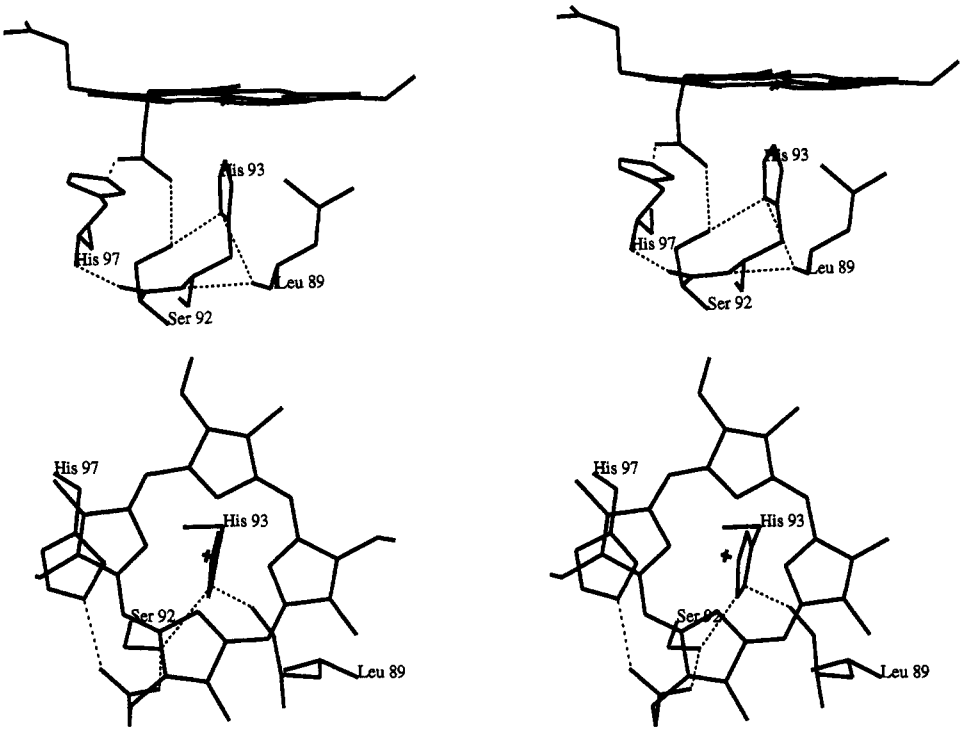

FIGURE 1: Approximately orthogonal stereoviews of the proximal heme pocket in the pig aquometmyoglobin crystal structure. Hydrogen bonding/electrostatic interactions are represented by dashed lines. (Top) View looking sideways into the heme pocket from the solvent-exposed face of the heme showing the proximal residues leucine[89], serine[92], histidine[93], and histidine[97]. (Bottom) View from the distal pocket looking onto the porphyrin and illustrating the eclipsed conformation of the imidazole ring of histidine[93] with respect to the pyrrole nitrogens. The network of hydrogen-bonding and electrostatic interactions, involving the proximal histidine[93], serine[92], leucine[89], the heme-7-propionate, and histidine[97], stabilizes the structure so that the proximal histidine is buried within the protein.

The orientation of the proximal histidine[97] side chain in lupin leghemoglobin is quite different with the plane of the imidazole ring staggered by close to 45° with respect to the pyrrole nitrogens (Vainshtein, 1981). This staggered conformation may well be an important determinant of the dramatically higher association rate and equilibrium constants for leghemoglobins compared to those for mammalian myoglobins (Mims et al., 1983; Gibson et al., 1989). The absence of a hydrogen bond between the proximal histidine imidazole group and the F7 side chain is presumably one of the factors governing the altered side-chain stereochemistry. In lupin leghemoglobin the F7 residue is valine[96], so that the N_δ-H group of the F8 imidazole makes a single hydrogen bond with the carbonyl oxygen of leucine[93] (F4). Threonine and serine residues are conserved at the F7 positions in the 71 vertebrate myoglobin sequences in the Swissport data base. In contrast, in the seven leghemoglobin sequences examined, this residue is valine or isoleucine. To define the role of the hydroxyl group of residue F7 in myoglobin, we have introduced alanine, valine, and leucine replacements into the pig protein and characterized these mutants structurally and functionally. The alanine replacement serves simply to remove the hydrogen-bonding group, while valine and leucine are the corresponding residues in lupin leghemoglobin and the human hemoglobin chains, respectively.

MATERIALS AND METHODS

Mutagenesis and Expression. Methods for overexpression and purification of recombinant pig myoglobin from *Escherichia coli* and the construction of site-directed mutants of the protein have been described previously (Dodson et al., 1988; Carver et al., 1991). The entire coding sequence of each of the three mutant myoglobin genes was determined to establish that no additional mutations had been introduced inadvertently. N-Terminal sequencing of the Leu[92] mutant myoglobin was carried out by Dr. K. S. Lilley, University of Leicester, as described by Matsudaira (1987).

Kinetic Measurements. Association and dissociation rate constants were measured for the binding of O_2, CO, and methyl and ethyl isocyanide ligands to the wild-type and mutant proteins according to the methods described by Rohlfs et al. (1990). Association equilibrium constants were calculated as the ratio of the association and dissociation rate constants. It has previously been demonstrated that recombinant pig myoglobin exhibits ligand binding properties identical to those of the native protein isolated from pig heart tissue (Carver et al., 1991).

Protoheme mono-3-(1-imidazoyl)propylamide monomethyl ester was prepared by Dr A. J. Mathews following the procedures of Traylor et al. (1979). In order to prepare solutions, a small amount of dried material was dissolved in ~0.05 mL of methanol to give a hemin concentration of 1–2 mM. Then, 10–50 μL of this solution was injected into phosphate buffer containing 2% by weight of myristyl trimethylammonium bromide [see Olson et al. (1983)].

The assay for hemin dissociation is being developed at Rice by M. S. Hargrove, L. Ortiz, E. W. Singleton, and J. S. Olson and has not been published. Following the procedures of Egeberg et al. (1990), His[64] was replaced with Tyr in sperm whale myoglobin to produce a mutant protein with a green color in the oxidized state at neutral pH. The abnormal spectral characteristics of the Tyr[64] myoglobin are due to direct coordination of the phenol side chain with the oxidized iron atom (Egeberg et al., 1990). The green color is due to an intense high-spin charge transfer absorption band at 600 nm compared to the weaker 630-nm band in native aquometmyoglobin. In addition, the Soret band of the mutant is blue-shifted from 408 to 410 nm compared to the wild-type protein.

Thus, when an excess of Tyr^{64} apoprotein is mixed with native or other mutant myoglobins, substantial absorbance changes occur as hemin is transferred to the protein containing a distal tyrosine. Under conditions of excess apoprotein, the observed first-order rate appears to represent the rate of hemin dissociation from the original holoprotein. The double mutant His → Tyr^{64}, Val → Phe^{68} was constructed in an attempt to stabilize the apoprotein for prolonged incubation at room temperature and to increase its affinity for hemin. In the experiments with position 92 mutants, ~5 μM myoglobin was mixed with excess Tyr^{64}-Phe^{68} apoprotein and the absorbance changes were monitored continuously in a Shimadzu 2101 UV–vis spectrophotometer equipped with a six-cell changer and a thermoelectric temperature control device (CPS-260). The buffer used was 0.2 M sodium acetate, pH 5.0.

Crystallography. Crystals of the Leu^{92} mutant myoglobin were grown under conditions identical to those used for the wild-type protein (Dodson et al., 1988). Three-dimensional X-ray data were collected from a single crystal at two settings on a Xentronics/Nicolet area detector device using a rotating anode source. Data were processed using the XDS package (Kabsch, 1988). The R_{merge} on intensities for 23 394 observations of 12 063 unique reflections was 4.6% to a nominal d_{min} = 2.7 Å. Effects of the Ser^{92} → Leu substitution were inferred initially from difference Fourier maps calculated with coefficients $F_{o_{mutant}} - F_{c_{wild\text{-}type}}$ or $F_{o_{mutant}} - F_{o_{wild\text{-}type}}$ with a phase set calculated from the model of the wild-type protein previously refined at 1.75-Å resolution (Oldfield et al., 1992). The initial crystallographic R-factor was 26.2% for all data.

The starting model for refinement was the coordinate set 1myg.pdb, deposited in the Brookhaven Protein Data Bank, with the side chains of residues $serine^{92}$ and $histidine^{97}$, the heme propionates, the sulfate ion, and water molecules in the vicinity the heme pocket set to zero occupancy. Refinement was carried out in three steps, each comprising manual model-building into electron density maps in the program FRODO and five cycles of positional and two cycles of temperature factor refinement using the program PROLSQ (Hendrickson & Konnert, 1979). This lowered the R-factor to 19.3% for all data between 10- and 2.6-Å spacing. Prior to the first cycle of restrained B-factor refinement, the B-values were truncated. Tight weighting of the geometrical terms relative to the X-ray terms (3:1–6:1) was maintained throughout the refinement steps. In the first rebuilding session, the heme-6-propionate, the side chains of $histidine^{97}$, and Cβ of $leucine^{92}$ were modeled into the electron density. Some 80 water molecules, for which no electron density was apparent, were taken out of the structure, and side chains poorly defined in $2F_o - F_c$ density were also set to zero occupancy. In subsequent rebuilds, attempts were made to position the heme-7-propionate and the $leucine^{92}$ side chain satisfactorily.

RESULTS

Expression and Purification. As described previously, wild-type pig myoglobin was overproduced in *E. coli*, as a fusion with the N-terminal 31 amino acids of λ cII protein (Dodson et al., 1988). Following reconstitution with exogenous heme, the fusion protein was digested with trypsin to yield intact holoprotein. The mutant proteins described in this study were prepared and purified following identical procedures. All three of the F7 mutants exhibited higher mobility than the wild-type protein on SDS–polyacrylamide gels following the proteolytic cleavage step. Further steps were therefore taken for the $leucine^{92}$ mutant to establish the integrity of the protein.

Table I: Kinetic Parameters for the Binding of O_2, CO, and Methyl and Ethyl Isocyanide to Wild Type and the Position[92] Ferrous Pig Myoglobin Mutants at 20 °C, pH 7

ligand	mutant	k' (μM^{-1} s^{-1})	k (s^{-1})	K_a (μM^{-1})
O_2	Ser^{92} (wild type)	17	14	1.2
	Ala^{92}	22	15	1.5
	Val^{92}	23[a]	4.6	5.0[a]
	Leu^{92}	24	5.5	4.5
CO	Ser^{92} (wild type)	0.78	0.019	41
	Ala^{92}	1.1	0.019	57
	Val^{92}	1.9	0.012[a]	160[a]
	Leu^{92}	1.8	0.012	150
MNC[b]	Ser^{92} (wild type)	0.11	4.4	0.025
	Ala^{92}	0.18	2.8	0.064
	Val^{92}	0.19	0.80	0.24
	Leu^{92}	0.17	0.97	0.18
ENC[b]	Ser^{92} (wild type)	0.10	0.63	0.15
	Ala^{92}	0.16	0.50	0.32
	Val^{92}	0.20	0.10	2.0
	Leu^{92}	0.18	0.19	1.0

[a] The time courses for O_2 association with Val^{92} myoglobin were heterogeneous, whereas those for O_2 dissociation were monophasic. The value of k'_{O_2} was computed from the half-times of the association time courses [i.e., $k'_{O_2} = \ln 2/(t_{1/2}[O_2])$]. Thus the association rate and equilibrium constants for this mutant are approximate. The opposite effect was observed for CO binding. The time course for CO association was monophasic whereas that for CO dissociation was biphasic, so that the k_{CO} and K_{CO} values are approximate. [b] Since high concentrations of isocyanide cause the binding of a second ligand, the rate and equilibrium parameters for formation of monomethyl and monoethyl isocyanide were derived from measurements at ligand concentrations ≤10^{-4} M. Even with this precaution, the parameters are approximate. Although the values of k' for the monoisocyanide complexes are accurately determined from analysis of the fast phases in the association reactions, the dissociation rate constants may contain contributions from dissociation of the diisocyanide complex.

Four cycles of Edman degradation performed on a sample of the Leu^{92} preparation yielded the sequence Gly-Leu-Ser-Asp, confirming that the mutant fusion protein had been appropriately cleaved to give the authentic pig myoglobin N-terminus. The presence of the authentic C-terminus and the integrity of the Leu^{92} mutant myoglobin polypeptide were established by determining the crystal structure of the Leu^{92} mutant as described below. Thus, the anomalous mobility on SDS–polyacrylamide gels is not a consequence of a lower molecular weight and remains unexplained.

Ligand Binding Kinetics. The rate and equilibrium constants for the binding of the ferrous ligands O_2, CO, and methyl and ethyl isocyanide were measured by stopped-flow rapid mixing and flash-photolysis experiments, and the results are summarized in Table I. The most striking observation is that the affinity of each of the mutant proteins is increased for all four ligands. The association equilibrium constants are increased between 1.3- and 13-fold in the mutants relative to the wild-type protein with the larger effects observed for the isocyanide ligands. For the Ala^{92} mutant the effects are consistently smaller than those for the Val^{92} and Leu^{92} mutants. In general, the dissociation rate constants are lowered, implying that the iron–ligand bonds have been strengthened. For the diatomic ligands, the changes in the O_2 association rate constants are modest compared to the changes observed for CO binding. This is a manifestation of the differing rate-limiting steps for the binding of these ligands. For oxygen, the bimolecular process of diffusion into the distal heme pocket from the bulk solvent is partially rate-limiting in the wild-type protein, whereas for CO association, unimolecular combination of the ligand with the iron from within the distal pocket is rate-limiting (Carver et al., 1990, and references therein).

Table II: Azide Binding Parameters for the Wild Type and Position[92] Ferric Myoglobin Mutants Measured at 20 °C in 0.1 M Phosphate Buffer, pH 7[a]

ligand	mutant	k' (M^{-1} s^{-1})	k (s^{-1})[b]	K_a (μM^{-1})[b]
N_3^-	Ser^{92} (wild type)	9800	0.18	0.05
	Ala^{92}	4800	0.037	0.13
	Val^{92}	2000	0.012	0.17
	Leu^{92}	3000	0.030	0.10

[a] Association reactions were carried out in the stopped-flow apparatus by mixing NaN_3 with 5 μM metmyoglobin and following the absorbance changes at 405 nm. Dissociation reactions were followed by replacing bound azide in the presence of excess NaCN. [b] The azide dissociation reactions for the mutants were markedly biphasic. The majority of the absorbance charge (60–80%) occurred slowly at the rates listed under k in the table. The initial phase exhibited a rate that was 100-fold greater and suggestive of cyanide binding to either free hemin or hemin weakly associated with denatured apoprotein. However, until the exact cause of the rapid phase is ascertained, the values of k and K_a for azide binding need to be viewed as equivocal.

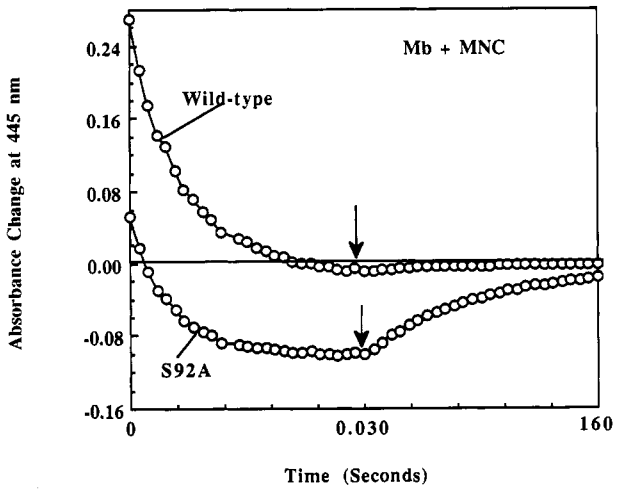

FIGURE 2: Time courses for the reaction of wild-type and Ala^{92} (S92A) pig deoxymyoglobin with 1 mM methyl isocyanide (MNC) in 0.1 M phosphate buffer, pH 7.0, 20 °C. The heme concentrations after mixing were ~5 μM and the wavelength of observation was 445 nm. The absorbance changes were collected on two time scales, 0–0.03 s and 0.03–160.03 s. The change in time scale is marked by the arrows. The symbols represent observed data and lines were drawn between the points. Both time courses could be fitted to the sum of two exponentials. The fitted first-order rate constants for the fast phases were 120 and 190 s^{-1} for wild-type and Ala^{92} pig myoglobin, respectively. The slow phase for the Ala^{92} mutant gave a fitted rate constant equal to 0.02 s^{-1}, whereas the slow phase for the wild-type protein was too small to allow an accurate rate constant determination.

The rate and equilibrium constants for the binding of azide to the ferric form of the wild-type and mutant proteins are presented in Table II. As for the ferrous ligands, an apparent in the ligand binding affinity is observed for all three mutant proteins. This is brought about by large 5–15-fold decreases in the dissociation rates for azide which more than offset the 2–5-fold decreases in the association rate constants. However, an exact interpretation is precluded by the heterogeneity observed in the dissociation time courses (see footnote b, Table II).

Stopped-flow time courses following the mixing of each of the mutants with methyl isocyanide show markedly biphasic kinetics at millimolar concentrations of ligand (Figure 2). In the initial phase there is a decrease in the A_{445} which takes place with a half-time of 5–10 ms; this is followed by a slow phase in which the absorbance at this wavelength increased with a half-time of 40–60 s. Qualitatively similar traces were produced for ethyl isocyanide (data not shown). As shown in Figure 2, significant slow phases were not observed for

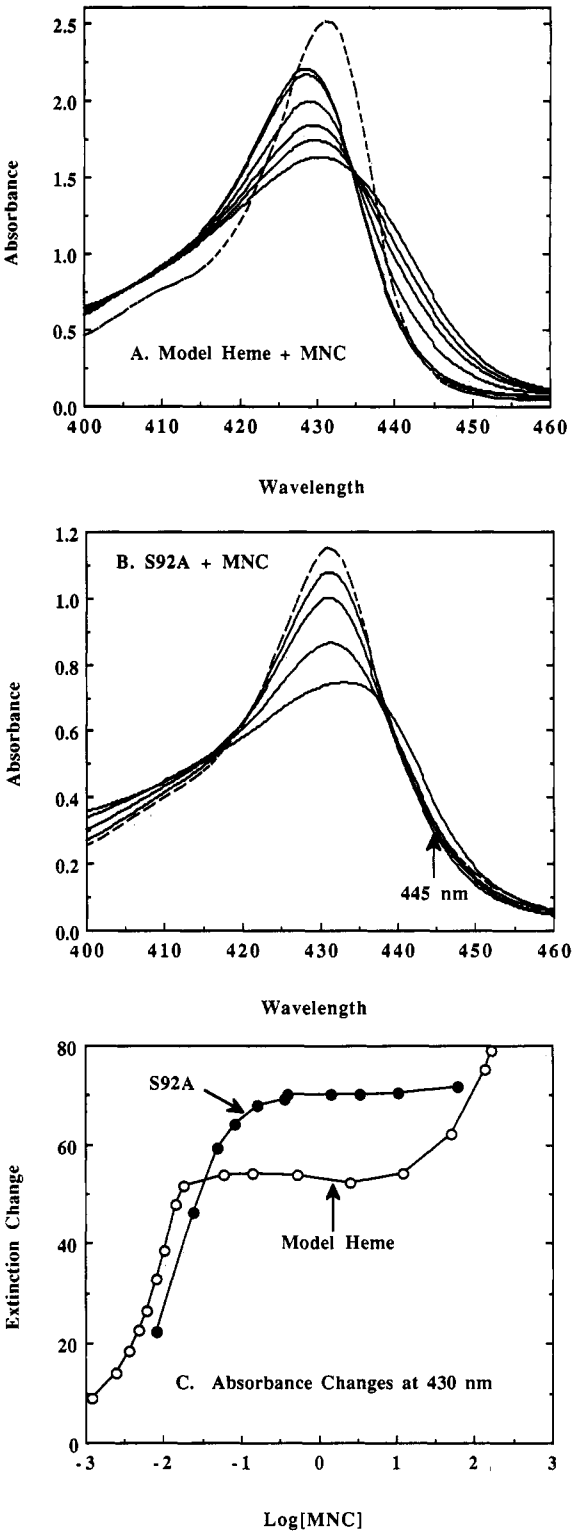

FIGURE 3: Equilibrium binding of methyl isocyanide to chelated protoheme and Ala^{92} (S92A) pig myoglobin at pH 7.0, 20°C. (Panel A) Titration of 12 μM chelated protoheme in 2% soap micelles and 0.1 M phosphate buffer. The solid lines represent spectra recorded after the incremental addition of 0–15 μM methyl isocyanide. The dashed line represents the spectrum of the sample after the addition of a total of 170 mM methyl isocyanide. (Panel B) Titration of 5 μM Ala^{92} pig myoglobin. The solid lines represent spectra recorded after the incremental addition of 0–80 μM methyl isocyanide. The dashed line represents the spectrum recorded after the addition of 60 mM ligand. (Panel C) Plot of the extinction change at 430 nm versus the logarithm of the total concentration of methyl isocyanide added to each sample in panels A and B. As shown, the formation of the mono- and diisocyanide-chelated protoheme complexes occur at widely separated ligand concentrations (micromolar vs millimolar), whereas these processes appear to be concerted for the Ala^{92} mutant.

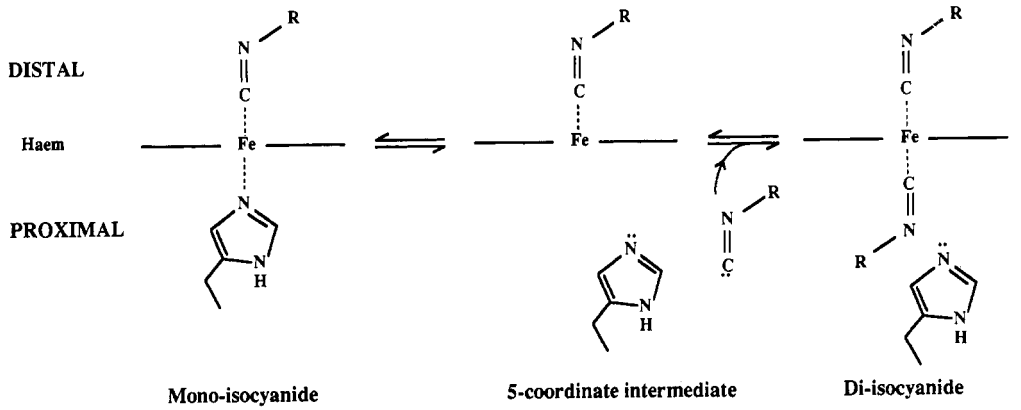

FIGURE 4: Schematic diagram of the mechanism of formation of the diisocyanide-liganded species. The iron–proximal histidine bond dissociates to give a transient 5-coordinate intermediate which then combines with a second isocyanide ligand (RNC).

wild-type pig myoglobin nor for the series of distal pocket mutants that we have examined previously (Rohlfs et al., 1990; Carver et al., 1991; Smerdon et al., 1991).

Similar, slow absorbance increases at 440–450 nm have been observed by us and others when chelated model hemes are reacted with high concentrations of isocyanides [T. E. Carver, A. Pham, and J. S. Olson, unpublished; similar "base-off" reactions were reported by Traylor and Stynes (1980)]. The effect with model hemes suspended in soap micelles is observed at millimolar concentrations for long-chain alkyl isocyanides, which accumulate preferentially in the hydrophobic micelle interior (Olson et al., 1983). An example of this behavior is shown in Figure 3 for protoheme mono-3-(1-imidazoyl)propylamide monomethyl ester suspended in 2% myristyl trimethylammonium bromide in 0.1 M sodium phosphate, pH 7.0, 20 °C. When low concentrations of methyl isocyanide are added to the deoxy form of chelated protoheme, the absorption maximum increases in intensity and is blue-shifted (431 to 428 nm) as the monomethyl isocyanide complex accumulates (solid lines, Figure 3A). When 10^{-2}–10^{-1} M methyl isocyanide is added, the absorbance maximum is red-shifted while the absorbance value at the maximum continues to rise (Figure 3A,C). The latter spectral changes are associated with the displacement of the imidazole and its replacement with a second isocyanide ligand to give the diisocyanide complex (Figure 4). Titration of the Ala^{92} mutant with methyl isocyanide does not show a clear transition from the mono- to diisocyanide adduct (Figure 3B,C).

Hemin Dissociation. The binding of a second isocyanide to the heme iron atom implies that the position 92 substitutions increase the accessibility of the proximal side of the heme group to ligands and solvent, weakening the strength of the Fe–His^{93} bond and decreasing the affinity of these proteins for the prosthetic group. This interpretation was tested directly by mixing the ferric forms of mutant and wild-type pig myoglobins with an excess of sperm whale Tyr^{64}-Phe^{68} apoprotein at pH 5.0, 20 °C (Figure 5). The time course for the appearance of "green" sperm whale metmyoglobin is governed by the rate of hemin dissociation from the pig proteins. As shown in Figure 5, the rates of hemin dissociation from the Ala^{92} and Leu^{92} mutants are 10–20 times greater than that for wild-type pig myoglobin. At higher pH values, the rates of hemin dissociation are much slower and therefore more difficult to measure accurately at 20 °C, particularly for the wild-type protein.

Crystal Structure. The initial impetus for determining an X-ray crystal structure of one of the mutants was to establish whether a C-terminal truncation had occurred in the course of the trypsin cleavage of the fusion protein. The presence

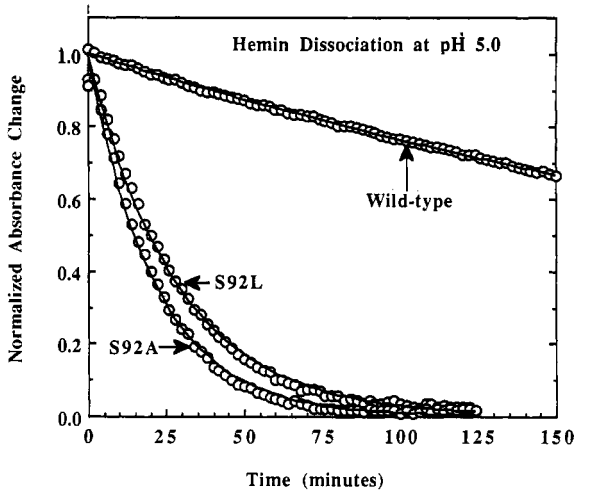

FIGURE 5: Time courses for hemin dissociation from wild-type, Ala^{92} (S92A), and Leu^{92} (S92L) pig metmyoglobin in 0.2 M sodium acetate buffer at pH 5.0, 20 °C. Approximately 5 μM pig myoglobin was mixed with 100 μM Tyr^{64}-Phe^{68} sperm whale apomyoglobin. The absorbance change for hemin transfer was followed at 408 nm and then normalized. The open circles represent observed data and the lines represent fits to a single exponential function. The observed rates were 0.0027 min^{-1}, 0.035 min^{-1}, and 0.047 min^{-1} for wild-type, Leu^{92}, and Ala^{92} pig myoglobin, respectively.

of an authentic C-terminus in the Leu^{92} mutant was confirmed by examination of difference electron density maps calculated with amplitudes and phases from a model in which the C-terminal three residues were omitted from the coordinate set and the structure was subjected to five cycles of positional refinement. Main-chain electron density extends to the C-terminal residue Gly^{153} even though, as for the wild-type and a series of mutant myoglobins, residues Gln^{152} and Gly^{153} are somewhat disordered.

The initial difference Fourier ($F_{o_{Leu92}} - F_{o_{wt}}$) maps reveal that the only significant positive and negative signals appear in the vicinity of the F7 side chain. Centered on the Oγ group of serine^{92} is a negative peak in the map, with an adjacent positive peak pointing away from the proximal imidazole that is most likely associated with the isobutyl side chain of the leucine replacement (Figure 6). The additional positive and negative peaks in this region of both molecules of the asymmetric unit provide clear evidence that the replacement of serine with leucine also causes significant perturbations of the stereochemistry of adjacent groups. There are prominent peaks in $F_{o_{Leu92}} - F_{o_{wt}}$ maps, contoured at -4σ, at the positions of the heme-7-propionic acid carboxylate group and the imidazole side chain of His^{97}. There are corresponding positive peaks in maps contoured at $+4\sigma$ (Figure 6). The positions

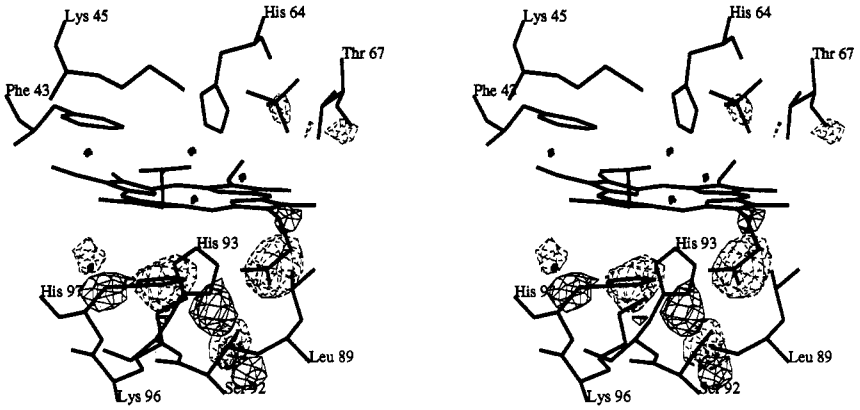

FIGURE 6: Electron density from the initial $F_{o_{mut}} - F_{o_{wt}}$ maps contoured at $+4\sigma$ (thin lines) and -4σ (broken thin lines) superimposed on the structure of wild-type pig myoglobin (thick lines). The figure shows the solvent-exposed face of the heme pocket of the A molecule. The asterisks represent either solvent water molecules or the iron atom at the center of the porphyrin ring. The sulfate ion present in the wild-type protein crystals is also shown. There are no other significant peaks in these maps elsewhere in the structure. The maps are very strikingly similar in the corresponding region of the B molecule.

of each of these peaks and their sizes are remarkably similar in both molecules of the asymmetric unit. The model has been refined by conventional cycles of least-squares minimization procedures (Hendrickson & Konnert, 1979) with sessions of manual model-building focusing on the proximal pocket region. The final structural model has an *R*-factor of 19.3% and decent stereochemistry, $rms_{bond} = 0.017$ and $rms_{angle} = 0.059$. The final electron density maps do not allow the heme-7-propionate carboxylate or the Cβ methyl substituent groups of leucine[92] to be positioned unambiguously in either the A or the B molecule, and these atoms are assumed to be disordered.

Taken together, the data suggest that a concerted series of structural changes has been brought about as a consequence of the removal of the hydrogen-bonding group at position[92]. As a result of the loss of the charge–dipole interaction between the heme-7-propionate and the F7 side chain, it appears that the former is no longer tethered to the proximal face of the heme pocket and has become disordered. In addition the interaction between N_ϵ of histidine[97] and the carboxylate oxygen of the heme-7-propionate is lost and there is a rotation of the histidine side chain about its Cα–Cβ bond so that the imidazole ring moves away from the C-terminus of the F helix. As a consequence, the proximal heme pocket and the proximal histidine have increased solvent exposure.

DISCUSSION

Site-directed mutagenesis experiments have defined the importance of polarity, hydrogen bonding, and steric hindrance in the distal pocket in ligand binding to hemoglobin and myoglobin. Proximal effects which influence the reactivity of the iron are likely to be more subtle and less easy to pinpoint from the crystal structures of these proteins, because small changes in the iron's atomic position could result in significant changes in its reactivity. The data presented in this paper demonstrate that the reactivity of the iron in pig myoglobin is influenced by the contact made to the imidazole ring of the iron-coordinating histidine[93] by the hydroxyl group of serine[92]. Replacement of the hydroxymethyl side chain of serine with the methyl, isopropyl, and isobutyl side chains of alanine, valine, and leucine, respectively, leads to increases in the association equilibrium constants for all of the ligands tested. The ligand affinities of the mutant proteins do not, however, approach those of leghemoglobin. They are rather more similar to the affinities of the isolated α and β chains of human hemoglobin, which both possess a leucine at the F7 position and bind ligands more tightly than wild-type myoglobin (Mims et al., 1983).

In contrast to the ferrous ligand binding kinetics, the rates of azide association with the ferric forms of the mutant proteins are slower than for the wild-type protein. The rate-determining step in azide binding is the displacement of the coordinated water in mammalian aquometmyoglobins. In *Aplysia* myoglobin, there is no iron-coordinated water at pH 6, and as a result the rates of azide association are 1000-fold faster than in mammalian myoglobins (Giacometti et al., 1981a,b). For a distal pocket pig myoglobin mutant, Val[68] → Thr, there is a marked reduction in the azide association rate constant that is attributable to the stabilization of the Fe-bound water by an additional hydrogen-bonding interaction with the Thr[68] OH group (Smerdon et al., 1991). The decrease in the rate of association of azide with the Ser[92] mutants strongly suggests that the affinity of the heme iron for water is also higher in these mutants. Thus, replacement of serine[92] with apolar residues leads to tighter binding of all ligands, ferrous as well as ferric. These effects suggest that the iron is intrinsically more reactive as a consequence of removal of the hydrogen bond between the proximal histidine and serine[92]. The uniform increase in the ligand binding affinities that arises from mutagenesis of a proximal residue seen here contrasts with the effects of distal pocket mutations, which invariably have discriminatory effects on ligands of different sizes and chemical characteristics (Olson et al., 1988; Springer et al., 1989; Carver et al., 1992).

It is possible that the eclipsed orientation of the plane of the proximal histidine imidazole with respect to the porphyrin nitrogen atoms modulates the chemistry of the heme iron by sterically restricting its movement into the plane of the porphyrin ring upon ligation and that this restriction is partially relaxed as a consequence of the mutations. However, no obvious rotation of the His[93] imidazole is seen in the X-ray structure of the aquomet form of the leucine[92] mutant. This may simply be a reflection of the fact that small changes in the orientation of the imidazole group, undiscernible at 2.7-Å resolution, give rise to the observed kinetic changes. It is clear, however, that the proximal imidazole ring in these mutants does not take up the staggered conformation observed in leghemoglobin. Alternatively, the observed kinetic changes may be due to subtle changes in the heme orientation that stem from the loss of the interaction between Ser[92] and the heme-7-propionic acid group.

The X-ray crystal structure of the Leu^{92} metmyoglobin mutant does show that there are substantial alterations to the proximal heme pocket. The imidazole group of the iron-coordinated histidine^{93} is buried in the wild-type protein by histidine^{97}, serine^{92}, the heme-7-propionate, and leucine^{89}. The serine to leucine^{92} mutation clearly destabilizes the interactions among these residues; the histidine^{97} imidazole is rotated away from the C-terminus of the F-helix, the heme-7-propionate has become disordered, and the position^{92} side chain no longer points in toward the proximal histidine. As a result there is a considerable increase in the solvent accessibility of the proximal histidine. There are two functional consequences of the disorder at the heme periphery which is introduced by aliphatic substitutions at position 92. The first is the increased accessibility of the proximal histidine to displacement by a second isocyanide ligand. The second is the 10–20-fold higher rate of hemin dissociation observed for the Ala^{92} and Leu^{92} mutants compared to wild-type pig myoglobin. This latter effect contributes to the instability of these proteins and probably accounts for the major portion of the selective pressure to conserve Thr or Ser at position 92 in mammalian myoglobins.

ACKNOWLEDGMENT

We should like to thank Drs. Peter Moody and Madeleine Moore for help in X-ray data collection and processing and Dr. C. Verma for technical assistance.

REFERENCES

Carver, T. E., Rohlfs, R. J., Olson, J. S., Gibson, Q. H., Blackmore, R. S., Springer, B. A., Egeberg, K. D., & Sligar, S. G. (1990) *J. Biol. Chem. 265*, 20007–20020.

Carver, T. E., Olson, J. S., Smerdon, S. J., Krzywda, S., Wilkinson, A. J., Gibson, Q. H., Blackmore, R. S., Ropp, J. D., & Sligar, S. G. (1991) *Biochemistry 30*, 4697–4705.

Carver, T. E., Brantley, R. E., Singleton, E. W., Arduini, R. M., Quillin, M. L., Phillips, G. N., & Olson, J. S. (1992) *J. Biol. Chem. 267*, 14443–14450.

Dodson, G. G., Hubbard, R. E., Oldfield, T. J., Smerdon, S. J., & Wilkinson, A. J. (1988) *Protein Eng. 2*, 233–237.

Egeberg, K. D., Springer, B. A., Martinis, S. A., Sligar, S. G., Morikis, D., & Champion, P. M. (1990) *Biochemistry 29*, 9783–9721.

Evans, S. V., & Brayer, G. D. (1990) *J. Mol. Biol. 213*, 885–897.

Giacometti, G. M., Ascenzi, P., Bolognesi, M., & Brunori, M. (1981a) *J. Mol. Biol. 146*, 363–374.

Giacometti, G. M., Ascenzi, P., Brunori, M., Rigatti, G., Giacometti, G., & Bolognesi, M. (1981b) *J. Mol. Biol. 151*, 315–319.

Gibson, Q. H., Wittenberg, J. B., Wittenberg, B. A., Bogusz, D., & Appleby, C. A. (1989) *J. Biol. Chem. 264*, 100–107.

Hendrickson, W. A. & Konnert, J. H. (1979) in *Biomolecular Structure, Conformation, Function and Evolution* (Srinivasan, R., Ed.) Vol 1, pp 43–57, Pergamon, New York.

Kabsch, W. (1988) *J. Appl. Crystallogr. 21*, 916–924.

Liddington, R., Derewenda, Z., Dodson, G., & Harris, D. (1988) *Nature 331*, 725–728.

Matsudaira, P. (1987) *J. Biol. Chem. 262*, 10035–10038.

Mathews, A. J., Rohlfs, R. J., Olson, J. S., Tame, J., Renaud, J.-P., & Nagai, K. (1989) *J. Biol. Chem. 264*, 16573–16383.

Mathews, A. J., Olson, J. S., Renaud, J.-P., Tame J., & Nagai, K. (1991) *J. Biol. Chem. 266*, 21631–21639.

Mims, M. P., Porras, A. G., Olson, J. S., Noble, R. W., & Peterson, J. A. (1983) *J. Biol. Chem. 258*, 14219–14232.

Nagai, K., Luisi, B., Shih, K., Miyazaki, G., Imai, K., Poyart, C., DeYoung, A., Kuriatkowsky, L., Noble, R. W., Lin, S.-H., & Yu, N. T. (1987) *Nature 329*, 858–860.

Oldfield, T. J., Smerdon, S. J., Dauter, Z., Petratos, K., Wilson, K. S., & Wilkinson, A. J. (1992) *Biochemistry 31*, 8732–8739.

Olson, J. S., McKinnie, R. E., Mims, M. P., & White, D. K. (1983) *Biochemistry 105*, 1522–1527.

Olson, J. S., Mathews, A. J., Rohlfs, R. J., Springer, B. A., Egeberg, K., Sligar, S. G., Tame, J., Renaud, J.-P., & Nagai, K. (1988) *Nature 336*, 265–266.

Perutz, M. F. (1970) *Nature 228*, 726–739.

Rohlfs, R. J., Mathews, A. J., Carver, T. E., Olson, J. S., Springer, B. A., Egeberg, K. D., & Sligar, S. G. (1990) *J. Biol. Chem. 265*, 3168–3176.

Scheidt, W. R., & Chipman, D. M. (1986) *J. Am. Chem. Soc. 108*, 1163–1167.

Smerdon, S. J., Dodson, G. G., Wilkinson, A. J., Gibson, Q. H., Blackmore, R. S., Carver, T. E., & Olson, J. S. (1991) *Biochemistry 30*, 6252–6260.

Springer, B. A., Egeberg, K. D., Sligar, S. G., Rohlfs, R. J., Mathews, A. J., & Olson, J. S. (1989) *J. Biol. Chem. 264*, 3057–3060.

Traylor, T. G., & Stynes, D. V. (1980) *J. Am. Chem. Soc. 102*, 5939–5941.

Traylor, T. G., Chang, C. K., Seibel, I., Berginis, A., Mincey, T., & Cannon, J. (1979) *J. Am. Chem. Soc. 101*, 6716–6731.

Vainshtein, B. K. (1981) in *Structural studies on molecules of biological interest* (Dodson, G., Glusker, J. P., & Sayre, D., Eds.) Clarendon Press, Oxford, England.